

Positioning and Immobilization of Individual Quantum Dots with Nanoscale Precision

Chad Ropp,[†] Zachary Cummins,[‡] Roland Probst,[‡] Sijia Qin,[§] John T. Fourkas,^{*,§,||} Benjamin Shapiro,^{*,‡} and Edo Waks^{*,†,⊥,#}

[†]Department of Electrical and Computer Engineering, [‡]Fischell Department of Bioengineering, [§]Department of Chemistry and Biochemistry, ^{||}Institute for Physical Science and Technology, [⊥]Institute for Research in Electronics and Applied Physics, and [#]Joint Quantum Institute, University of Maryland, College Park, Maryland 20742, United States

ABSTRACT We demonstrate a technique for the precise immobilization of nanoscale objects at accurate positions on two-dimensional surfaces. We have developed a water-based photoresist that causes nanostructures such as colloidal quantum dots to segregate to a thin layer at surfaces. By combining this material with electroosmotic feedback control, we demonstrate the ability to position selected, individual quantum dots at specific locations and to immobilize them with 130 nm precision via localized UV exposure.

KEYWORDS Quantum dots, deterministic assembly, electroosmotic flow, feedback control

The ability to place nanoscopic objects at precise locations on patterned or prepared surfaces is essential for a broad range of device applications. One important example is the positioning of quantum dots (QDs) in nanophotonic structures such as cavities^{1–3} and waveguides⁴ for single-photon generation,^{5–7} quantum dot lasers,⁸ or nonlinear optical devices.⁹ Another example is the nanoscale positioning of metallic and dielectric particles on prepared metamaterial surfaces to engineer nanoscopic electronic circuits.¹⁰ The majority of these applications exploit optically resonant interactions that require the nanoscopic particles to have the correct spectral properties. For these applications, it is essential to have a technique that can preselect the particles with the correct spectral properties and place them at the correct locations on a surface.

The positioning of preselected particles with nanometric precision is an extremely difficult task with few good solutions. Optical tweezers are a widely utilized technique for nanometer scale particle manipulation.^{11,12} However, optical gradient forces scale with particle volume, making it difficult to trap nanoscopic objects.¹³ In addition, these traps also do not ensure single particle manipulation since they are nonspecific and will acquire multiple particles over time.¹² Other techniques that make use of mechanical manipulators have also been used to push, pull, and place individual metal and dielectric nanoparticles on a variety of surfaces.^{14–17}

In this paper, we demonstrate a broadly applicable method for positioning and immobilization of nanoparticles in precise locations on a surface. This method takes advantage of electroosmotic flow control (EOFC), a technique that we have recently demonstrated for the accurate, nanoscale

positioning of nanoparticles.¹⁸ In EOFC, particle positioning is achieved by controlling the flow of the surrounding fluid and feedback is used for the continuous correction of the position of a chosen nanoparticle. Previous demonstrations of flow control have achieved manipulation of micrometer-sized particles with micrometer precision,^{19–21} random capture of nanoparticles with nanometric holding accuracy,^{22–24} and more recently manipulation of nanoparticles with nanometric precision.¹⁸

A major limitation of EOFC to date has been that actuation of individual particles can only be achieved in two of three dimensions, since fluid flow occurs only along the directions that lie parallel to the fluid channels. Thus, a particle that is being manipulated on the bottom surface of the device is free to diffuse out of plane, making it difficult to place the particle on a prepatterned surface. Another important limitation is that all particles in the device are subject to flow. Therefore, once a desired particle has been positioned, it is not possible to manipulate a second particle without disturbing the position of the first one.

Here, we demonstrate a method that overcomes both of these difficulties. The specific nanoparticles that we manipulate are colloidal cadmium selenide quantum dots (QDs). Single QDs are generally difficult to manipulate due to their small sizes and sensitivity to their physical environment. However, QDs are exceptionally interesting for nanophotonics and quantum optics applications in which they can serve as bright sources of single photons. QDs also play an important role in biological applications as tags and markers.²⁵ To achieve manipulation and immobilization of individual QDs along a surface we have developed a water-based, negative-tone photoresist that causes QDs to be localized within a thin sheath along the surfaces of a microfluidic channel. When using this photoresist, EOFC of the nanoparticles occurs effectively in two dimensions at the surface of interest. After the QD has been delivered to a desired

* To whom correspondence should be addressed. E-mail: (E.W.) edowaks@umd.edu; (B.S.) benshap@umd.edu; (J.F.) fourkas@umd.edu.

Received for review: 08/20/2010

Published on Web: 10/06/2010

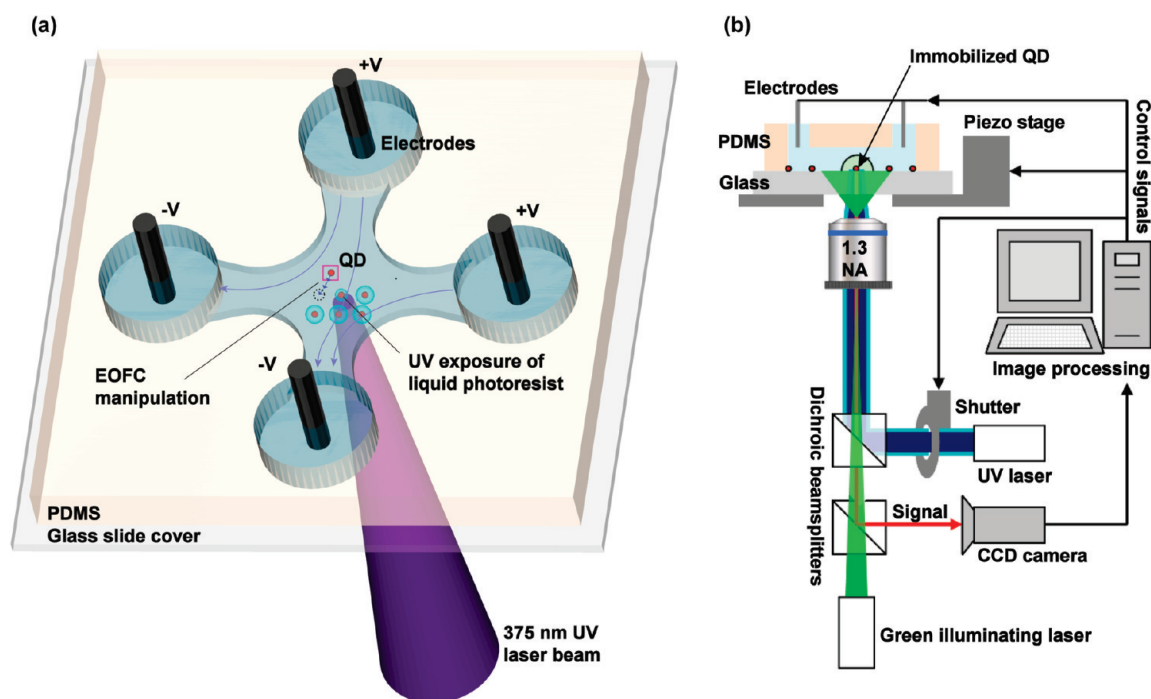


FIGURE 1. Microfluidic device and setup. (a) The microfluidic device is formed between a glass cover slide and a molded PDMS block. Colloidal CdSe/ZnS QDs are suspended in the photoresist, which is used to fill the device. Electrodes placed in the four fluid reservoirs provide the voltages necessary to move QDs as desired using EOF. A UV laser is integrated to expose the photoresist at a central location in the setup. This location can be moved by translating the sample stage. (b) Experimental setup showing a cross section of a microfluidic channel. Dichroic beam splitters are used to integrate the UV source for photoresist exposure and the green source for illumination. Signals from the QDs are filtered and imaged on a CCD camera. Data collected from the camera are analyzed through image processing to determine the location of the QDs. The desired feedback signals are calculated and then sent to the electrodes, the piezo stage, and the UV shutter to coordinate the positioning.

location by EOF, a brief exposure to ultraviolet light polymerizes the surrounding fluid to immobilize the QD. Once a selected QD has been immobilized, manipulation of subsequent QDs will not affect its position. This technique makes possible the sequential, high-precision positioning and immobilization of a large number of selected nanoparticles on a 2D surface.

A schematic of the microfluidic device used in our experiments is shown in Figure 1a. The device is composed of a pair of microfluidic channels formed between a glass coverslip and a molded block of polydimethylsiloxane (PDMS). The control region resides at the intersection of the two channels and has a width of $100\ \mu\text{m}$ and a height of $5\ \mu\text{m}$. The microfluidic channels are filled with a mixture of QDs (Invitrogen Qtracker PEG CdSe/ZnS 655 nm) suspended in an aqueous photoresist we have developed. The photoresist is composed of a water-soluble multifunctional acrylic monomer, a radical photoinitiator, and a rheology modifier used to increase fluid viscosity. A detailed description of the resist is provided in the Supporting Information. When exposed to UV light, the photoresist will cross-link in the exposed area to form a small polymerized region that can be used to encapsulate and immobilize a QD. The monomer is added at a concentration near its solubility limit, which causes the QDs to segregate to the surfaces of the device, as shown and discussed in detail in the Supporting Information. Four

electrodes are immersed in the fluid reservoirs, providing the voltages necessary for EOF.²⁶ These electrodes can actuate the buffer to flow in any of the four cardinal directions parallel to the glass substrate.

Figure 1b shows a diagram of the experimental setup, which consists of an inverted confocal microscope that images the QDs onto a CCD camera operating at a 10 Hz frame rate. QDs are illuminated with a 532 nm laser at $100\ \text{W}/\text{cm}^2$. Individual QDs are tracked in real time by the imaging system. Subpixel averaging, based on a centroid estimate, is used to determine the position of a QD to a precision that is much better than the diffraction limit of the optical system²⁷ (see Figure S1 in the Supporting Information). Once the position of a QD is determined, a control algorithm applies voltages to the four electrodes to actuate the correcting electroosmotic flow.¹⁹ The control algorithm applies the voltages needed to move the QD from its current location toward the target location via a continuous control loop, quickly driving the position error down to a limit set by the imaging accuracy and particle diffusion between control updates.²⁰

Figure 2 shows how QDs that have been pushed to the surfaces of the device can be manipulated along the surface by electroosmotic actuation. The chosen QD is selected by our control software²¹ and moved toward the specified location, as shown in Figure 2a–c. We observe a strong blinking

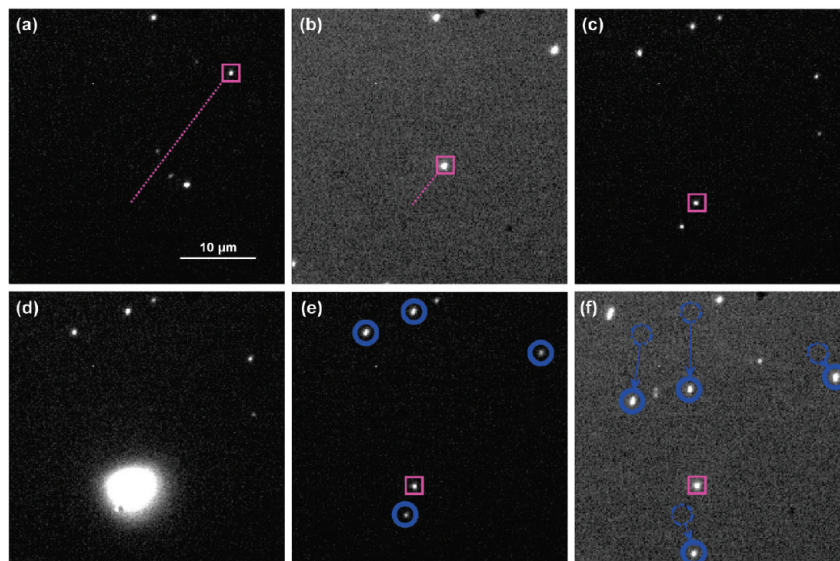


FIGURE 2. Positioning and immobilization of a single QD. (a–c) A single QD is chosen (magenta box) and moved toward the target location. The line shows the distance between the QD and the target. (d) Image showing the local UV exposure, aligned with the target location, used to immobilize the QD once it is in place. (e,f) After the QD is encapsulated (magenta box) it does not move with an applied voltage to the South electrode, although the QDs in the surrounding solution do move. Several other QDs are circled in blue (e) and their displacements after one second of flow are shown in panel (f).

behavior, which is evidence that we are indeed manipulating single QDs (definitive proof that we are manipulating single QDs is obtained by performing photon antibunching measurements, as discussed in the Supporting Information). The control algorithm performs actuation only when the QD is in the luminescent state, as determined by a threshold value for its observed intensity. Once the QD is at the target position, the area containing the QD is irradiated by a 375 nm laser beam that is centered on the target position to achieve local cross-linking of the photoresist. The UV laser is focused to a spot size of $2\ \mu\text{m}$ with an intensity of $500\ \text{W}/\text{cm}^2$. A shutter is triggered automatically to expose with UV light for 400 ms (Figure 2d) once the QD is determined to be within 80 nm of the target position. Figure 2e,f shows successive camera frames obtained after the QD was immobilized. A voltage was applied on the north electrode to create electroosmotic actuation in the south direction. As can be seen from these two frames, the immobilized QD remains at the same position while the surrounding QDs move with the flow.

The ability to position and immobilize nanoparticles opens up the possibility for assembling complex patterns of preselected QDs. As an example, we created a 3×3 square lattice array of QDs with $5\ \mu\text{m}$ separation between adjacent lattice sites. A single QD was first positioned and immobilized at a desired location near the center of the control area. A piezo stage was then used to move the sample to the next location in the array, where the next QD was subsequently positioned. A video of the array being assembled is available in the Supporting Information. Figure 3a shows the resulting 3×3 array. This image is an average of four consecutive frames, each with a 500 ms exposure time, and is displayed on an intensity-log scale. The leftmost QD in the middle row emitted

less brightly than the others during this exposure period, and so it appears dimmer in the image. The entire array was monitored over a period of 15 s and subpixel averaging was used to measure the position of every QD during frames in which they were in the luminescent state (Figure 3b). Figure 3c shows a zoomed-in plot of the measured positions for one of the QDs. These measured positions are all well localized. We note that there is a slight asymmetry between the variance in the x and y directions of the measured positions. This asymmetry is attributed to a small drift of the piezo stage over the measurement time.

Positions for each of the nine QDs were determined by averaging over each data set. We determined the vision accuracy of the subpixel averaging, based on the standard deviation of measured positions for each QD, to be 14 nm (8 nm) in the x (y) directions. To obtain a measure of the relative in-plane positioning precision for QD immobilization, we fit our data to an ideal $5\ \mu\text{m}$ grid by translating and rotating the data and optimizing the average distance between the two. When optimized, the average error in distance was measured to be 127 nm, which is our precision in reproducing the array on the surface.

A single image of the encapsulated QDs after channel removal is shown in Figure 3c on an intensity-log scale. All of the polymerized regions remained adhered to the slide surface, and several of the QDs (shown circled in red) can be seen clearly emitting at the correct locations even after channel removal. The remaining QDs were in a dark state during this particular frame. At other camera frames, these QDs became luminescent while some of the other QDs became dark. The data in Figure 3 demonstrate that devices can be assembled in a fluidic environment and then used once the channels have

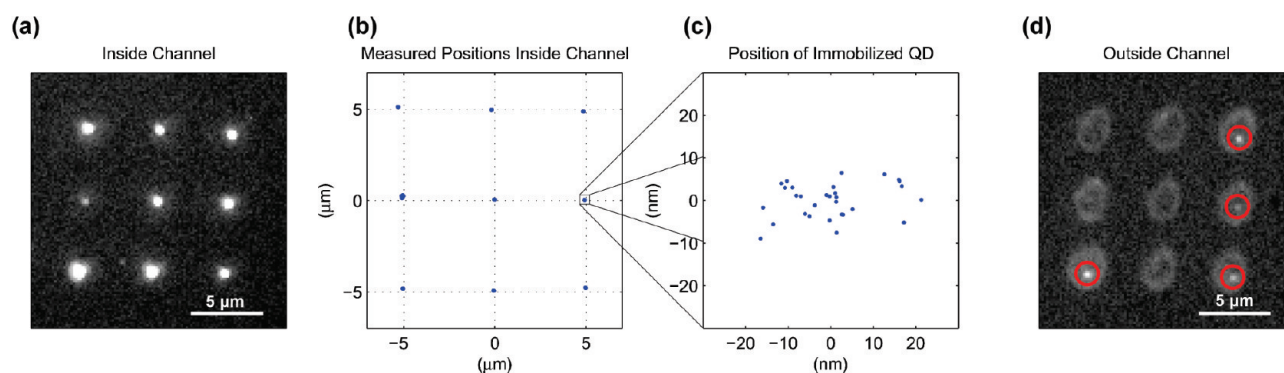


FIGURE 3. Immobilized array of individual QDs. (a) Image of the 3×3 array of immobilized QDs with $5 \mu\text{m}$ spacing within the microfluidic channel. (b) Measured positions of the nine QDs from averaging over many frames. (c) A zoomed-in view of the measured positions for the QD in the center-right of the array with the origin corresponding to its mean position. (d) Image of the 3×3 array after channel removal and cleaning, demonstrating that several of the QDs are still emissive. All of the exposed regions have remained adhered to the glass surface (seen as oval-shaped bright patches) and the four luminescent immobilized QDs are shown circled in red.

been removed. We note that a degradation in emission brightness of the QDs is observed after channel removal. The cause of this emission degradation is not fully understood but may be due to oxidation during assembly and cleaning. Methods for reducing this contamination using oxygen scavengers have been investigated previously and could serve to reduce QD degradation significantly.²⁸ We also note that the polymerized regions shown in Figure 3d are on the order of $2\text{--}3 \mu\text{m}$ in diameter. Such large polymerized regions are not suitable for applications requiring close packing of many nanoscopic particles. These spot sizes could be reduced with improved focusing of the UV beam and could potentially be made much smaller (sub 100 nm diameter) using multiphoton absorption polymerization.^{29,30}

To measure the distance of the immobilized QDs from the surface, we exploited the fact that a small fraction of QDs adhere to the surface naturally in the course of an experiment. These adhered QDs serve as reference points that enable us to determine the position of the glass surface. We positioned and immobilized three QDs in a $20 \times 20 \mu\text{m}$ area that contained three naturally adhered QDs. This small region was chosen to minimize systematic errors in depth measurements due to nonuniformity of the surface and to spherical aberrations in the microscope. The distance between the objective lens and the surface was then varied by moving the piezo stage in and out of focus in steps of 200 nm . Both the immobilized and naturally adhered QDs were imaged for many frames at each stage position and the sizes of the diffraction spots were tabulated using the variances of the QD image. For every QD, a median diffraction spot size was calculated at each position and the data were fit to a beam divergence function of the form³¹

$$w(z) = w_0 \sqrt{1 + \left(\frac{z - z_0}{z_R}\right)^2} \quad (1)$$

where w represents the width of the diffraction spot as a function of focus position z . The minimal diffraction spot size

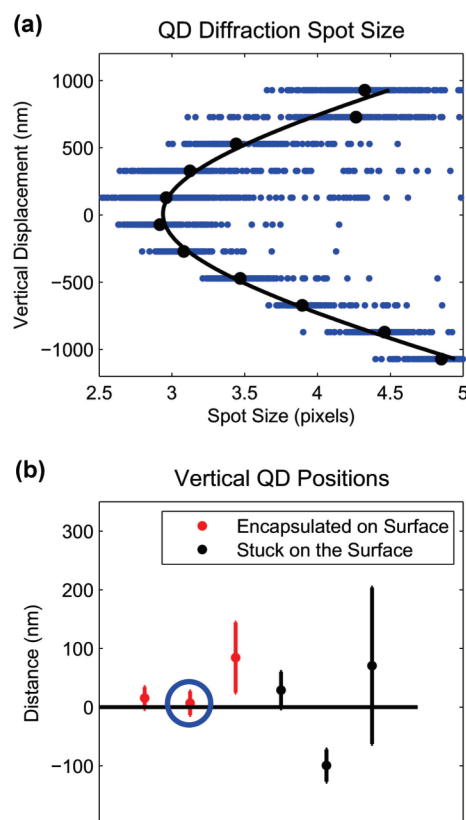


FIGURE 4. Proximity of QDs to the surface. (a) Graph of the diffraction spot size of an encapsulated QD at varied focal distances from the surface. At each position the diffraction spot size was measured many times (blue data points) and a median size (black points) was calculated. A fit was used to find the location of the minimum spot size (black line), establishing the vertical position of the QD. (b) Measured in-focus vertical positions of three encapsulated QDs (red) and three QDs adhered to the surface (black) with corresponding error bars. The blue circle denotes the QD corresponding to measurements shown in panel a.

denoted by w_0 is located at the vertical position z_0 . The Rayleigh range of the diverging spot is z_R . A plot of the diffraction spot size, in pixels, of one of the encapsulated QDs as a function of focal depth is shown in Figure 4a. The

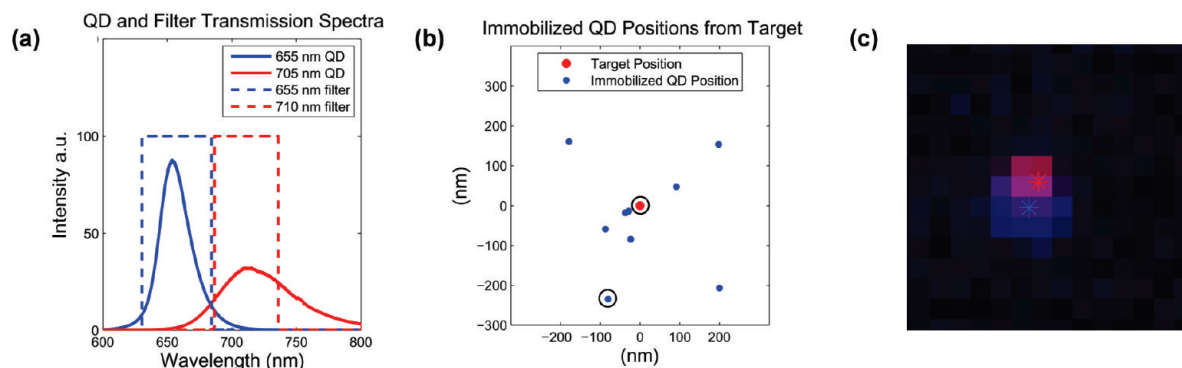


FIGURE 5. Immobilization of individual QDs to target QDs adhered to the substrate. (a) Spectra of the two different types of QDs and the bandpass transmission spectra of the two filters used to distinguish between them. (b) Relative positions of the nine positioned and immobilized QDs that emit at 655 nm (blue dots) versus their 705 nm targets (all marked by a single red dot at the origin). The average distance between the immobilized QDs and their adhered QD targets was measured to be 155 nm. The two circles denote the sample QD pair whose pixelated images are overlaid in panel (c), here the red and blue asterisk mark the location of the diffraction pattern centroids inferred by the subpixel averaging algorithm.

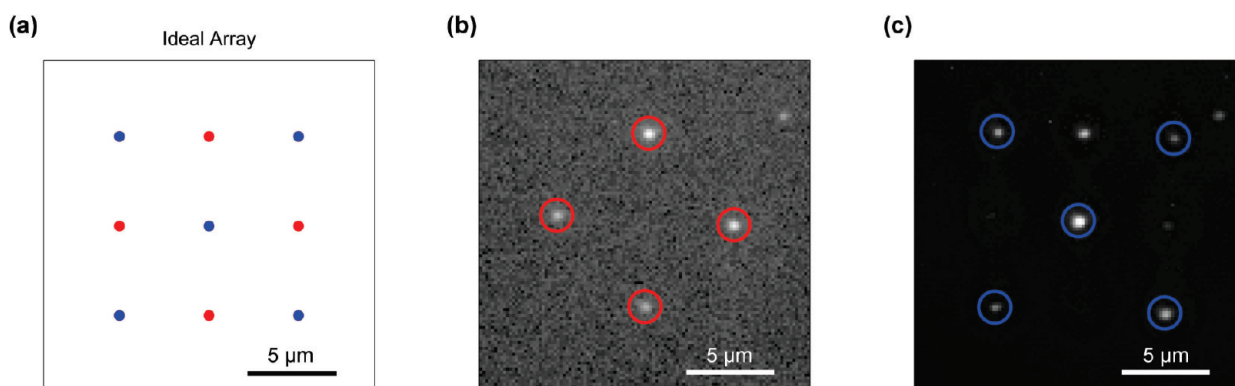


FIGURE 6. Array of preselected QDs. (a) Idealized array design with the two different types of QDs alternating in a checkerboard pattern. (b) Completed array as visualized through a bandpass filter centered at 710 nm. The four QDs emitting at ~ 705 nm are circled in red while the 655 nm emitting QDs are not visible. (c) The same completed array as visualized through the 655 nm band-pass filter. The QDs emitting at 655 nm are circled in blue.

fit was used to determine the location of the minimal diffraction spot (and hence the in-focus z position of the QD) from the fitting parameter z_0 . This procedure was carried out for the remainder of the QDs, and the results are shown in Figure 4b. The vertical positions of the naturally adhered QDs are shown in black and those of the immobilized QDs are shown in red. We denote the average position of the naturally adhered QDs as $z = 0$, the location of the glass surface. The position of this surface was determined with a standard deviation of 80 nm. The average position of the three encapsulated QDs is given by 35 ± 38 nm. The uncertainty in the vertical measurements of both the adhered and encapsulated QDs is likely caused by vision noise in our imaging setup, QD blinking, and the inherent roughness of the slide cover. The accuracy of the measurement could be improved significantly by using better methods for measuring the out-of-plane position of the QDs based on cylindrical lenses³² or a double helix point spread function.³³

To demonstrate that this positioning technique can deliver a QD to a marked location on a surface, we deposited a low concentration of a different species of QDs emitting at an average wavelength of 705 nm (Invitrogen Qtracker

PEG CdSe/ZnS 705 nm) onto a dry slide cover. These QDs, which remain adhered to the glass surface after filling the channels, served as targets. The channels were filled with the same 655 nm emitting QDs used in previous experiments. The two species of QDs can be distinguished visually by using bandpass filters centered at 655 and 710 nm, respectively, in front of the imaging camera. We measured the emission spectra of the two types of QDs using a grating spectrometer (Acton SP 2758 with a resolution of 0.06 nm). Figure 5a shows the measured emission spectra of bulk samples of both types of QD. Additionally, overlaid in Figure 5a are the transmission spectra of the bandpass filters, demonstrating that they can be used for selective visualization of the two different types of QDs.

Individual 705 nm emitting QDs served as stationary targets for the positioning and immobilization of 655 nm emitting QDs. Target QDs whose emission does not bleed through the 655 nm filter were chosen so that the tracker would not get confused between the two QD types while performing the positioning. Nine 655 nm QDs were immobilized on top of nine chosen 705 nm QD targets, and the positions of all of them were then measured using

subpixel averaging. In Figure 5b, the red dot at the origin marks the 705 nm target position for all nine pairs; the blue dots show the measured relative displacements of the nine placed and immobilized 655 nm QDs. The average distance between an immobilized QD and its target was calculated to be 155 nm. An overlapped diffraction image of one of the immobilized 655 nm QDs (blue) versus its 705 nm target QD (red) is shown in Figure 5c with an asterisk labeling their inferred centroid positions.

A unique feature of our positioning and immobilization technique is that it enables us to characterize QDs before they are immobilized. Thus, QDs with desired spectral properties can be preselected and delivered to specific locations on a device. As a demonstration of this capability, we fabricated a 3×3 array of QDs with different specified colors at each point (Figure 6a). To construct this complex structure, we injected a mixture of both the 655 nm emitting and the 705 nm emitting QDs. By alternating between filters after each immobilization step, we assembled a 3×3 array of color selected QDs in a checkerboard pattern. A video demonstrating how this technique is able to differentiate between the two types of QDs for immobilization is available for viewing in the Supporting Information.

Figure 6b,c shows the final assembled array as seen through the 710 and the 655 nm filters, respectively. The picture in Figure 6b was acquired in one image frame with a 500 ms exposure time, while the picture in Figure 6c was acquired from an average of many minutes of frames with 500 ms exposure times each in order to visualize all five of the QDs, which were never in the luminescent state simultaneously. The QDs that are expected to be seen based on the filter used are circled in each picture. With the 710 nm filter in place only the correct QDs are visible. However, the top-middle QD from the 705 nm batch is clearly visible through the 655 nm filter (Figure 6c), due to the fact that the 705 nm QDs have more inhomogeneous spectral broadening than do the 655 nm QDs (as seen in the spectra in Figure 5a). Therefore, a QD from the 705 nm sample is more likely to partially overlap with the passband of the 655 nm filter.

In conclusion we have demonstrated a method for positioning and immobilization of preselected nanoparticles along a two-dimensional surface. These results were achieved by combining high precision tracking and feedback control with the development of a water-based photoresist that restricts QDs to a thin sheath near the surface of a microfluidic channel. Here we have demonstrated the positioning of colloidal quantum dots, but the technique is general and can be employed with any nanoscopic particle that can be visualized. It is also potentially amenable to use with virtually any substrate that is compatible with water. This technique is a powerful new approach for the precision, high-yield assembly of complex nanostructures that combines the advantages of bottom-up and top-down nanofabrication.

Acknowledgment. This work was supported by a DARPA Defense Science Office grant (Grant W31P4Q0910013). E.W. acknowledges funding support from a National Science Foundation CAREER award (grant number ECCS - 0846494), the Physics Frontier Center at the Joint Quantum Institute, and the Office of Naval Research Applied Electromagnetics Center.

Supporting Information Available. Subpixel accuracy, photoresist chemistry, and autocorrelations of immobilized quantum dots. Also, movies showing the assembly of the 3×3 array corresponding to Figure 3 in the text and the technique of color discrimination are available. This material is available free of charge via the Internet at <http://pubs.acs.org>.

REFERENCES AND NOTES

- Badolato, A.; Hennessy, K.; Atature, M.; Dreiser, J.; Hu, E.; Petroff, P. M.; Imamoglu, A. *Science* **2005**, *308*, 1158–1161.
- Hennessy, K.; Badolato, A.; Winger, M.; Gerace, D.; Atature, M.; Gulde, S.; Falt, S.; Hu, E. L.; Imamoglu, A. *Nature* **2007**, *445*, 896–899.
- Englund, D.; Faraon, A.; Fushman, I.; Stoltz, N.; Petroff, P.; Vuckovic, J. *Nature* **2007**, *450*, 857–861.
- Wong, C.; Gao, J.; McMillan, J.; Sun, F.; Bose, R. *Photonics Nanostruct.* **2009**, *7*, 47–55.
- Michler, P.; Kiraz, A.; Becher, C.; Schoenfeld, W. V.; Petroff, P. M.; Zhang, L.; Hu, E.; Imamoglu, A. *Science* **2000**, *290*, 2282–2285.
- Santori, C.; Pelton, M.; Solomon, G.; Dale, Y.; Yamamoto, Y. *Phys. Rev. Lett.* **2001**, *86*, 1502.
- Yuan, Z.; Kardynal, B. E.; Stevenson, R. M.; Shields, A. J.; Lobo, C. J.; Cooper, K.; Beattie, N. S.; Ritchie, D. A.; Pepper, M. *Science* **2002**, *295*, 102–105.
- Huffaker, D. L.; Park, G.; Zou, Z.; Shchekin, O. B.; Deppe, D. G. *Appl. Phys. Lett.* **1998**, *73*, 2564.
- Fushman, I.; Englund, D.; Faraon, A.; Stoltz, N.; Petroff, P.; Vuckovic, J. *Science* **2008**, *320*, 769–772.
- Engheta, N. *Science* **2007**, *317*, 1698–1702.
- Ashkin, A.; Dziedzic, J. M.; Bjorkholm, J. E.; Chu, S. *Opt. Lett.* **1986**, *11*, 288–290.
- Jauffred, L.; Richardson, A. C.; Oddershede, L. B. *Nano Lett.* **2008**, *8*, 3376–3380.
- Dienerowitz, M.; Mazilu, M.; Dholakia, K. *J. Nanophotonics* **2008**, *2*, No. 021875.
- Miyazaki, H.; Sato, T. Proceedings of MEMS '96, San Diego, CA, February 11–15, 1996; IEEE: New York, 1996; pp 318–324.
- Chey, S. J.; Huang, L.; Weaver, J. H. *Appl. Phys. Lett.* **1998**, *72*, 2698–2700.
- van der Sar, T.; Heeres, E. C.; Dmochowski, G. M.; de Lange, G.; Robledo, L.; Oosterkamp, T. H.; Hanson, R. *Appl. Phys. Lett.* **2009**, *94*, 173104–3.
- Barth, M.; Schietinger, S.; Fischer, S.; Becker, J.; Nušse, N.; Aichele, T.; Löffel, B.; Soñnichsen, C.; Benson, O. *Nano Lett.* **2010**, *10*, 891–895.
- Ropp, C.; Probst, R.; Cummins, Z.; Kumar, R.; Berglund, A. J.; Raghavan, S. R.; Waks, E.; Shapiro, B. *Nano Lett.* **2010**, *10*, 2525–2530.
- Armani, M.; Chaudhary, S.; Probst, R.; Shapiro, B. 18th IEEE International Conference Micro Electro Mechanical Systems, Miami, FL, 2005; IEEE: New York; pp 855–858.
- Armani, M.; Chaudhary, S.; Probst, R.; Shapiro, B. *J. Microelectromech. Syst.* **2006**, *15*, 945–956.
- Probst, R.; Cummins, Z.; Shapiro, B. *Nat. Protoc.*, in press.
- Cohen, A. E. *Phys. Rev. Lett.* **2005**, *94*, 118102.
- Cohen, A. E.; Moerner, W. E. *Proc. Natl. Acad. Sci. U.S.A.* **2006**, *103*, 4362–4365.
- Cohen, A. E.; Moerner, W. E. *Opt. Express* **2008**, *16*, 6941–6956.
- Medintz, I. L.; Uyeda, H. T.; Goldman, E. R.; Mattoussi, H. *Nat. Mater.* **2005**, *4*, 435–446.

- (26) Probst, R. F. *Physicochemical hydrodynamics*; John Wiley and Sons: New York, 1994.
- (27) Thompson, R. E.; Larson, D. R.; Webb, W. W. *Biophys. J.* **2002**, *82*, 2775–2783.
- (28) Hohng, S.; Ha, T. *J. Am. Chem. Soc.* **2004**, *126*, 1324–1325.
- (29) LaFratta, C. N.; Fourkas, J. T.; Baldacchini, T.; Farrer, R. A. *Angew. Chem., Int. Ed.* **2007**, *46*, 6238–6258.
- (30) Maruo, S.; Fourkas, J. T. *Laser Photonics Rev.* **2008**, *2*, 100–111.
- (31) Siegman, A. E. *Lasers*; University Science Books: Sausalito, CA, 1986.
- (32) Kao, H. P.; Verkman, A. S. *Biophys. J.* **1994**, *67*, 1291–1300.
- (33) Pavani, S. R. P.; Thompson, M. A.; Biteen, J. S.; Lord, S. J.; Liu, N.; Twieg, R. J.; Piestun, R.; Moerner, W. E. *Proc. Natl. Acad. Sci. U.S.A.* **2009**, *106*, 2995–2999.

Positioning and Immobilization of Individual Quantum Dots with Nanoscale Precision

Chad Ropp[†], Zachary Cummins[‡], Roland Probst[§], Sijia Qin^{||}, John T. Fourkas^{||,&}, Benjamin Shapiro[‡], Edo Waks[†]

[†]Department of Electrical and Computer Engineering, [‡]Fischell Department of Bio-Engineering, [§]Department of Aerospace Engineering, ^{||}Department of Chemistry and Biochemistry and [&]Institute for Physical Science and Technology, University of Maryland, College Park, Maryland 20742, USA

Supporting Information

1. Subpixel Accuracy

Achievement of nanometric positioning and immobilization of single nanoparticles using our microscope setup requires us to be able to extract subwavelength-of-light information from an optical signal. To attain this goal we employ subpixel averaging, which requires that the diffraction spot of the imaged particle be spread out over several pixels on the imaging CCD. A center of mass of calculation of the image will measure the position of the particle at the center of its diffraction spot. The accuracy of this technique is fundamentally limited by the signal-to-noise ratio of the particle compared to the read and shot noise of the camera. However, the measurement accuracy gets better as this position is averaged over many frames. With this technique we are able to measure nanoscopic changes in position. To demonstrate the power of this technique, a single QD stuck on a slide cover was moved in increments of 24 nm using a piezo actuator while its position was measured continuously via our centroiding algorithm. The data is shown in Figure S1a. The incremental steps of 24 nm can be seen above the noise from the raw data (black), but the steps are especially visible when the positions are averaged over time (red). The measured average positions and the actual positions imparted by the piezo are displayed in Figure S1b, and show very good agreement. Therefore, we are able to perform

position measurements on immobilized QDs with high accuracy despite being limited to diffraction spot information from our nanoparticles.

2. Photoresist chemistry

The photoresist used in our experiments is composed of 0.6 wt% rheology modifier (Acrysol RM-825, Rohm and Haas Co.)¹, 40% by volume ethoxylated-15 trimethylolpropane triacrylate (SR-9035, Sartomer)², 0.3 wt% synthesized MBS photoinitiator³, and QDs with a molar concentration of 100 pM (Qtracker PEG CdSe/ZnS 655 nm) in deionized water. The monomer and photoinitiator provide the photocrosslinking capability, while the rheology modifier is used to increase the viscosity of the fluid and therefore reduce the Brownian motion of the colloidal QDs. The polymer also notably decreases QD surface binding.

The synthesis of the photoinitiator, sodium 4-[2-(4-Morpholino)benzoyl-2-dimethylamino]butylbenzenesulfonate (MBS), was performed with a modified version of a literature procedure³ (Figure S2). A solution 7.0 g of 2-benzyl-2-(dimethylamino)-1-(4-morpholinophenyl)-1-butanone (BDMB) in 10 mL of chloroform was added slowly to 24.4 g of fuming sulfuric acid under nitrogen with stirring. The sulfonation reaction proceeded exothermically.

After 2 hours of stirring, the reaction mixture was added slowly to 300 mL of deionized water. The solution was neutralized with 22.0 g of calcium hydroxide, and the calcium sulfate precipitate was filtered away. The precipitate was washed three times with 150 mL of deionized water and this liquid was added to the filtrate. Sodium carbonate (0.764 g) was then added to the filtrate, and the calcium carbonate precipitate was filtered off. The filtrate was then concentrated and dried.

Purification was accomplished by column chromatography on magnesium silicate with a 1:1 molar ratio of ethyl acetate and ethanol as the solvent. The water-soluble, purified MBS was collected as a pale yellow powder upon evaporation of the solvent. The overall yield was 71.4% (6.63 g).

All fluid components mix well with water except the monomer at this proportion. When the monomer is mixed an emulsion is formed that includes globules of fluid containing the colloidal QDs. These globules can be seen filling the microfluidic channel and adsorbing to the

surfaces within the devices. The resulting films of QDs in water still exhibit good EOFC and the QDs within these films do not show significant signs of surface binding or agglomeration. Figure S3 shows images of the filled microfluidic channel at different heights with (Figure S3a-c) and without (Figure S3d-f) the monomer added to the fluid. When the monomer is added the QDs are found to be dispersed only at the top PDMS surface (Figure S3a) and bottom glass surface (Figure S3c) of the devices. A large QD-containing globule can be seen in focus only in the middle of the cross channel (red in panel b). Figure S3b also distinctly shows QDs forming a thin film along the channel walls (blue), indicating that the QDs are coating all surfaces. These results can be compared to Figures S3d-f, which correspond to the situation in which there is no monomer. In this latter case, the QDs are equally dispersed throughout the microfluidic channel, as evidenced by the fact that the number of in-focus QDs is the same at each focal plane.

3. Autocorrelation of immobilized quantum dots

To ensure we are controlling and immobilizing single QDs, a 2×2 array of QDs was assembled (Figure S4a) and an autocorrelation measurement was performed on the encapsulated QDs while they were still inside the microfluidic channel. A small aperture was closed down along the beam for spatial filtering of the QD signal, which was then diverted into a Hanbury-Brown-Twiss (HBT) type autocorrelation setup consisting of a 50:50 beam splitter and two avalanche photodiodes set to count coincidence photons. The photodiodes were also gated so as not to accumulate counts when the QD is blinked off. Correlations were obtained over a one minute integration time. For these measurements, our pumping power was well below saturation. The normalized cumulative counts could be fit to a function of the form $g^2(\tau) = [1 - (1 - g^2(0))e^{-\Gamma_s\tau}]$, where Γ_s is the spontaneous emission rate of the QD. The resulting $g^2(\tau)$ measurements for each of the four immobilized QDs are shown in Figure S4b. The measured $g^2(0)$ s were found to be 0.29, 0.26, 0.26, and 0.35. All $g^2(0)$ s are well below 0.50, indicating that we are positioning only single photon emitters.

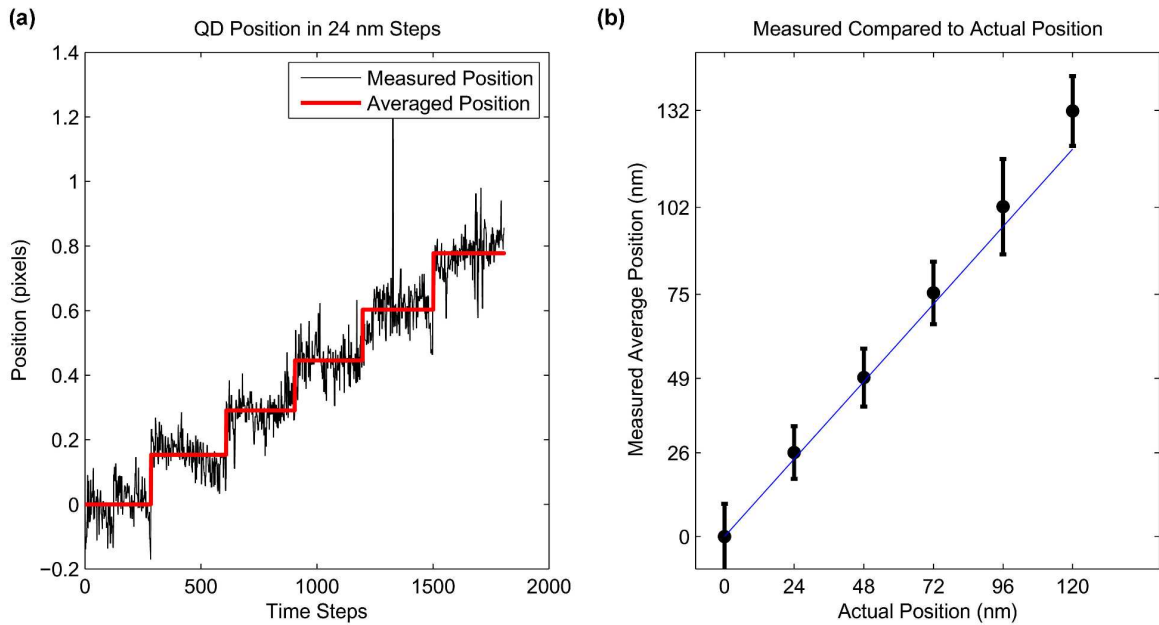


Figure S1. Measured position of a QD as the piezo stage was moved in 24 nm increments (a) Measured data showing the subpixel accuracy of our centroiding algorithm. The black data are the measured pixel position of the QD, while the red line is the average position for each step. Discrete steps are seen clearly in the measured data. (b) Measured average position (from panel a) showing the mean and standard deviation compared to the actual position imparted by the piezo stage when converted into actual length units. The blue line denotes when the measured position equals the actual position. In general the measurement has high accuracy and can easily distinguish changes in piezo displacement.

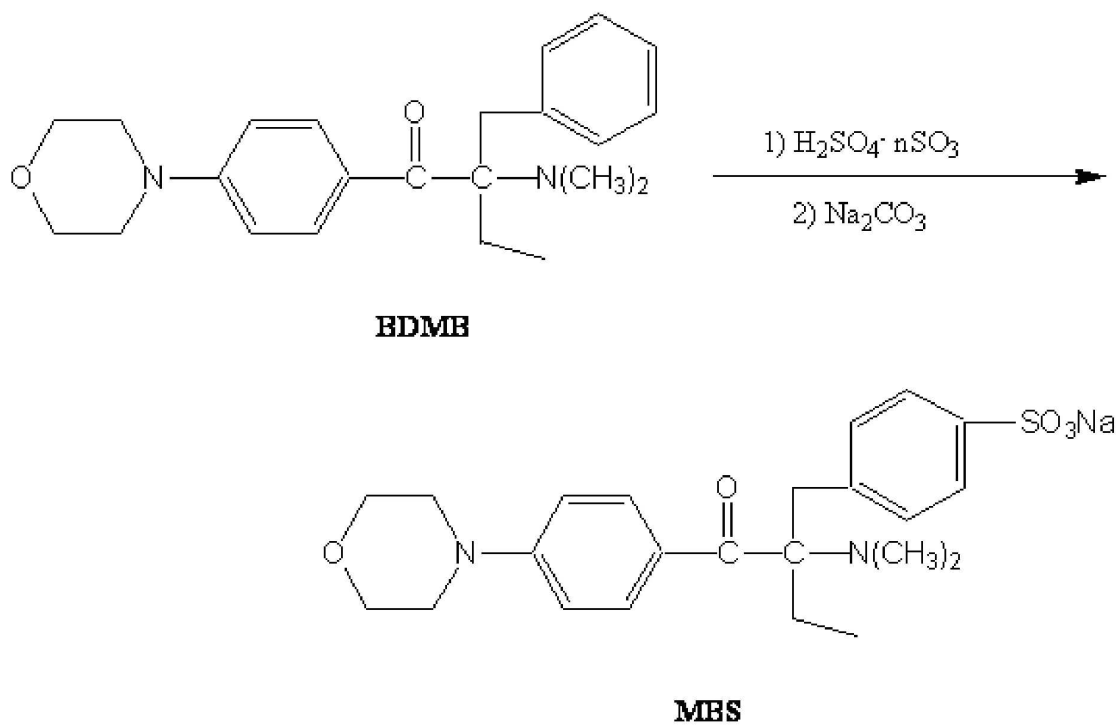


Figure S2. Synthetic scheme for the water-soluble radical photoinitiator MBS.

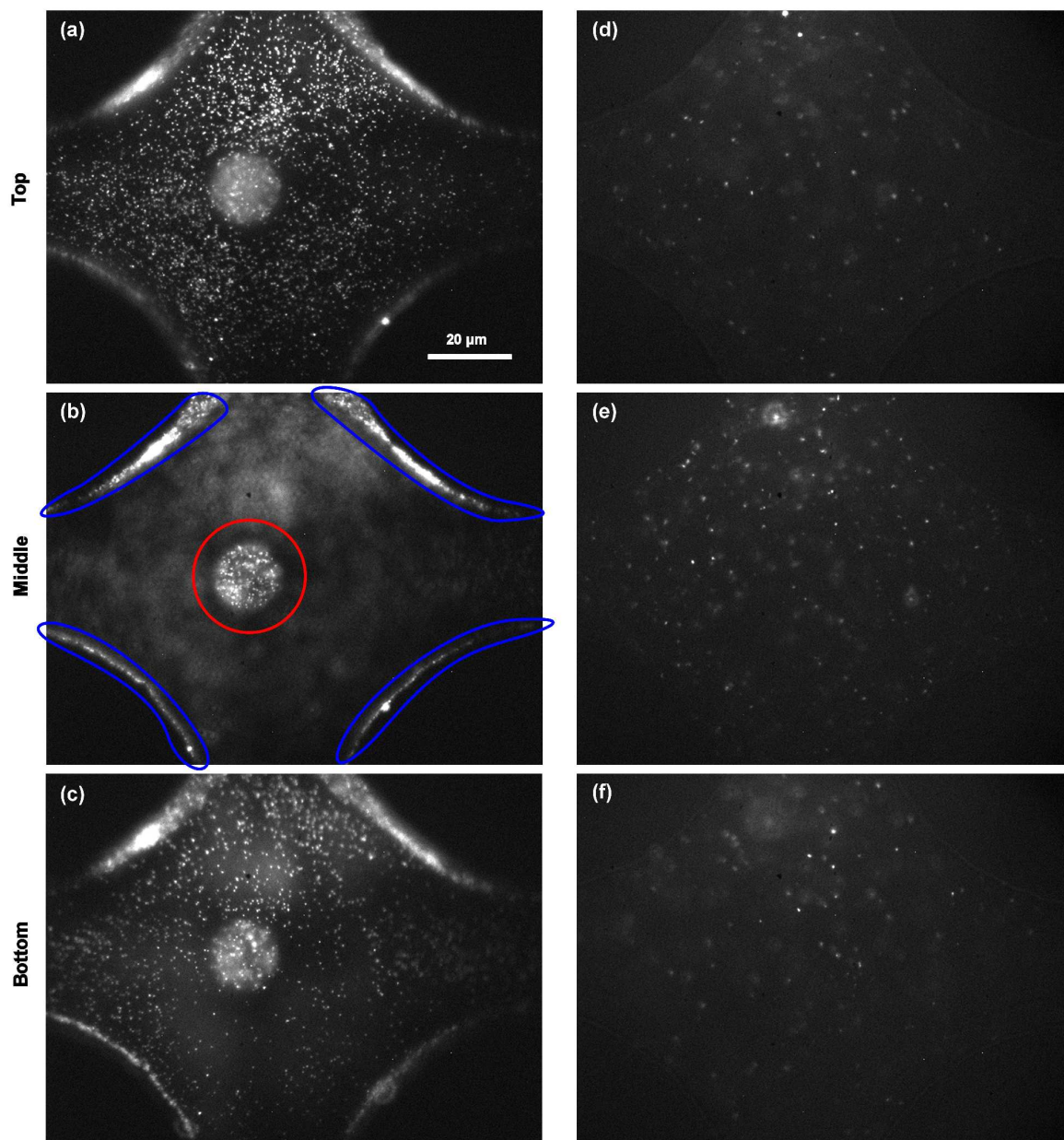


Figure S3. Images showing QD films along surfaces. (a-c) Microfluidic channel filled with rheology modifier and the immiscible monomer (0.6% RM-825 and 40% SR-9035) shown at different planes within the device. QDs in focus at both the top (PDMS) and bottom (glass) surfaces can be seen along with a large globule (red) and thin layers of QDs along the channel walls (blue) in the middle of the channel. (d-f) Microfluidic channel filled without the monomer (0.6% RM-825) at the same planes within the device. QDs are dispersed uniformly vertically throughout the device.

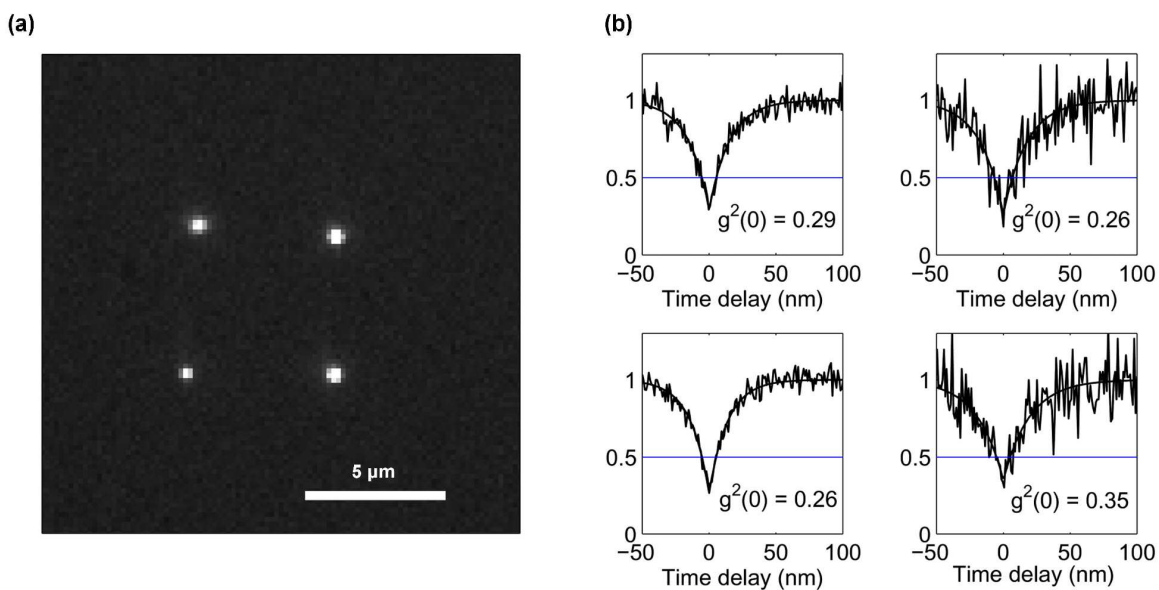


Figure S4. Array of immobilized dots and their measured $g^2(\tau)$ s. (a) Image of the 2×2 array of QDs spaced $5 \mu\text{m}$ apart. (b) The corresponding $g^2(\tau)$ measurements for each of the four respective QDs. Autocorrelations are taken over a 1 minute integration time while the QDs are still in the channel. The measured $g^2(0)$ s are 0.29, 0.26, 0.26, and 0.35 and all show signs of the photon antibunching that is characteristic to quantum emitters.

REFERENCES

- (1) Kumar, R.; Raghavan, S.R. *Langmuir* **2009**, in press.
- (2) Liu, J.; Gao, D.; Li, H.; Lin, J. *Lab. Chip* **2009**, *9*, 1301-1305.
- (3) Kojima, K.; Ito, M.; Morishita, H.; Hayashi, N. *Chem. Mater.* **1998**, *10*, 3429-3433.